Acoustic emission induced by progressive excavation of an underground powerhouse

AUTHOR(S):

Ishida, Tsuyoshi; Kanagawa, Tadashi; Uchita, Yasuo

Fault-Plane Solutions by Sensitive, High-Frequency Monitoring of Acoustic Emissions Induced by Progressive Excavation of an Underground Powerhouse

By Tsuyoshi Ishida[a]*, Tadashi Kanagawa[b] and Yasuo Uchita[c]

[a]Department of Civil and Earth Resources Engineering, Kyoto University, Katsura, Nishikyo-ku, Kyoto 615-8540, Japan.

(E-mail address: ishida.tsuyoshi.2a@kyoto-u.ac.jp)

[b]Central Research Institute of Electric Power Industry, Abiko, Chiba 270-1194, Japan.

(E-mail address: kana-gawa@jcom.home.ne.jp)

[c]Kansai Electric Power Company Co. Inc., Osaka 530-8270, Japan.

(E-mail address: k-daden@leto.eonet.ne.jp)

* Corresponding author. Tel.: +81-75-383-3209; fax: +81-75-383-3213

E-mail address: ishida.tsuyoshi.2a@kyoto-u.ac.jp (T. Ishida).

ABSTRACT

We monitored acoustic emission (AE) events associated with the progressive excavation of an underground chamber for a powerhouse at a depth of 280 m below the surface in a porphyritic rock mass of the Mesozoic era. Large AE events rarely occur under such conditions; specifically, low-stress environments due to the shallow depth, careful excavation, and sufficient reinforcement. However, upon employing sensitive, high-frequency monitoring (15 to 40 kHz) in a relatively small region, some AE events were located and, by using fault-plane solutions, their fracture mechanisms were identified. Strike and dip angles of fracture planes and the directions of principal stresses, all derived from fault-plane solutions, were consistent with the directions of dominant joint surfaces, the measured initial stress conditions, and the shape of nearby excavated openings. This suggests that by employing sensitive, high-frequency AE monitoring, fault-plane solutions can be effectively utilized as a tool to assess the stability of a chamber excavated at shallow depth, as well as in deep mines where fault-plane solutions have already been used in practice to assess and control rockbursts.

Keywords: Acoustic emission, Fault-plane solution, Underground powerhouse, Rock stress, Joint surface, Fracture.

1. INTRODUCTION

When excavating a large chamber such as one for an underground powerhouse, it is important to monitor the stability of the rock mass around the chamber being evacuated. Acoustic emission (AE) or microseismicity monitoring is a viable, nondestructive method for detecting microfracture prior to a macroscopic rock fracture. Even in cases where only P-wave data are available without corresponding S-wave data, we can locate an AE event by reading out the arrival times of P-wave first motions within recorded waveforms of the event. Furthermore, if we can distinguish the polarities of those P-wave first motions, we can discern the fracture mechanism of the AE event. In other words, from the polarities, we can distinguish whether P-wave arrivals at AE sensors are compressive or dilatational (respectively indicated as upward or downward traces on the recorded waveforms) and, from that, determine the strike and dip angle of the fracture plane accompanying the AE event and the directions of the principal stresses inducing the AE event. For example, should a numerical simulation suggest a possibility of a tensile fracture in a portion of an underground chamber, we can check for this risk by monitoring and analyzing AE events induced around that portion. As another example, should a large stress concentration be predicted, we can check whether such a stress concentration is actually induced; furthermore, we can also check whether the maximum stress direction is the same as that predicted, free of the influence of inherent joint orientations or other rock mass

inhomogeneity. A merit of AE monitoring is its ability to obtain information not only on fracture location, but also on fracture mechanism. Many other monitoring methods are unable provide such information.

With regard to induced seismicity in metal mines excavated from 1400 to 3500 m deep, fracture mechanisms are often identified by using the fault-plane solution and moment tensor inversion [1-3]. These methods are also applied to the identification of fracture mechanisms in coal mines, which have relatively shallow depths from 600 to 1500 m but also have much larger volume excavations, thereby inducing stress concentrations of the same approximate intensity as deep metal mines [4-6]. Nevertheless, with regard to large chambers excavated at a relatively shallow depth for civil engineering works (e.g., an underground powerhouse), the fracture mechanisms of AE events have been rarely identified, except for examples obtained in the closely monitored environment of the Underground Research Laboratory in Canada as reported by Young's research group [7-9]. The reason seems to be that AE events having enough energy to be located in three dimensions and to be analyzed for their fracture mechanism are only rarely induced in shallow chambers, which are typically characterized by low stress, careful excavation, and sufficient reinforcement. Now, however, considering that count rates and frequency changes of AE events have been successfully monitored and utilized in a chamber being evacuated for an underground powerhouse as reported by Cai et al. [10], we should be able to obtain valuable information on fracture

mechanisms and the like through sensitive monitoring of AE events.

We monitored AE events induced by the progressive excavation of an underground powerhouse chamber for the Ohkawachi Power Station in Hyogo Prefecture, Japan. The powerhouse is located at a depth of 280 m below the surface. As expected, large AE events were rarely encountered during excavation. However, by employing sensitive, high-frequency monitoring (15 to 40 kHz) for small AE events over a relatively small region (making use of experience accumulated through previous tests, including direct shear testing [11], small-scale in situ heater testing [12], and small-scale hydraulic fracturing testing [13]), we were able to locate several AE events in three dimensions and identify their fracture mechanism. The strike and dip angles of fracture planes and the directions of the principal stresses thus derived were consistent with the directions of dominant joint surfaces, measured initial stress conditions, and the shape of excavated openings near the location of an AE event. The results demonstrate that even with regard to chambers carefully excavated under low-stress conditions at a shallow depth and with sufficient reinforcement, AE monitoring can provide useful information for stability assessment. In this paper, we present and discuss data previously reported separately in earlier symposiums [14, 15] together with new data.

The monitoring itself was conducted in 1990, and thus the instruments used for the monitoring were outdated in comparison with

current technology. This said, the date of monitoring is not of any particular significance in relation to other aspects of this paper.

Back then, the Kansai Electric Power Company, which was responsible for power supply in the Kansai area (central Japan), faced a need to accommodate timing differences between electricity supply and demand peaks. The company moved to construct a pumped storage hydroelectric powerhouse, the Ohkawachi Power Station. The underground powerhouse was constructed as a part of the facility, with work beginning in March 1988 and ending November 1992.

During an era of rapid economic growth from 1970 to 1995, many underground powerhouses were constructed in Japan. In conjunction, many in situ measurements were carried out during excavation [e.g., 16, 17], with much data obtained on rock mass properties [e.g. 11]. These data have proved invaluable in investigations of rock-mass behavior and chamber wall fracture. Among such data, the AE monitoring data described in this paper are particularly well preserved and conveniently arranged for analysis. Here, we revisit the data to demonstrate the possibility of identifying microfracture mechanisms in a shallow chamber under low stress through the use of sensitive, high-frequency AE monitoring.

In this research, we used only P-wave first motions without S-waves. We do so because we cannot find S-wave arrivals in the traces, which are

superimposed with many other waves probably produced by reflections off chamber surfaces. We identified the fracture mechanism of an AE event using the fault-plane solution, rather than moment tensor inversion, which, in addition to the polarities of P-wave first motions, also requires their amplitudes. It is difficult to ensure equal sensitivity to amplitude across all sensors for two reasons: (i) within high-frequency monitoring (from 5 to 100 kHz, as employed here), the sensitivity of a sensor is not constant but depends strongly on the frequency; and (ii) we could not find a reliable method to calibrate the coupling effect between a sensor and cement in a borehole under high-frequency monitoring, a difficulty pointed out by Shah and Labuz [18] in their laboratory experiments. For these reasons, we considered the fault-plane solution to be much more suitable and reliable than moment tensor inversion for identifying the fracture mechanism.

2. MONITORING SITE

2.1. Outline

AE events were monitored during the progressive excavation of the main chamber for the powerhouse of the Ohkawachi Power Station, a pumped storage water power station in Hyogo Prefecture, Japan. Figure 1 shows the layout and two sectional views of the chamber, which, upon completion, measures 24.0 m wide, 46.6 m high, and 134.5 m long. It was excavated at a depth of about 280 m within a Mesozoic era porphyritic rock mass.

AE events were monitored from holes drilled in a chamber wall at a location not far from what would become the installation position for the No. 3 dynamo, near the center of the main chamber. Three AE monitoring holes were drilled prior to chamber excavation from a previously excavated magnetizing equipment room, as shown in Fig. 1. In addition to the AE monitoring holes, another hole, this one to hold a multi-extensometer for displacement measurement, was drilled at a 22 m horizontal distance from those holes (displacement measurement would later be used to verify fracture mechanisms against those deduced from monitored AE events).

The mechanical properties of the porphyritic rock are summarized in Table 1. Young's moduli obtained from drilled cores in a laboratory and from the rock mass in situ were 76 and 24 GPa, respectively. These values

are higher than the average moduli of rocks in Japan. In terms of the classification of the rock mass quality, *Q*, proposed by Barton et al. [19], the *Q* value was measured to range from 4 to 20, corresponding to 'Fair' to 'Good' in the classification.

2.2. Pre-existing joints and their orientations

Observations of drilled cores and video images obtained by a borehole television system show that, on average, the rock mass had 10 joints per meter. It was thus expected that the wall rock mass would not behave as a continuum. Another hole was drilled along the AE holes, and at 11 points along that hole we monitored the change in vertical diameter with progress of chamber excavation. As expected, the results suggested that stress redistribution with progressive excavation was strongly affected by this presence of many pre-existing joints [17].

Figure 2 shows a lower hemisphere projection of joint surface orientations on a Schmidt net. These joint surface orientations were measured in the AE holes before AE sensors were set in them. From the figure, we note that the most dominant joint surface (9 to 11% concentration) is around a point 68° clockwise from true north and 68° from the vertical.

2.3. In situ stress

Over-coring in situ stress measurements were conducted at the two

points using the two sets of the three holes, OC1, OC2 and OC3, and OC4, OC5 and OC6, drilled from investigation adits above the chamber (see Fig. 1). In the stress measurements, the multi-element (5 elements) strain gage developed by Kanagawa et al. [20, 21] was used. In the multi-element gage, four strain gauges are oriented in radial directions of the hole (at 45 degree intervals) and one strain gauge is directed axially. With these five strain gauge elements, the two-dimensional principal in situ stress condition in the radial plane and a normal stress component in the axial direction can be obtained. However, to determine the 3-dimensional in situ stress condition, it is necessary to carry out two set of over-coring in differently directed boreholes. In practice, it is better for accuracy to carry out the stress relief method in 3 boreholes oriented in different directions [20, 21, 22]. In the stress measurement, the 3 holes were drilled horizontally at 45 degrees intervals to determine the stress condition at each of the two points, and over-coring measurements were conducted three times along each hole.

Since the three dimensional stress conditions respectively obtained at the two points did not show large difference, average stress condition for the construction site was determined using all released strains in the six boreholes [23]. As shown in Figure 3, the magnitude of the maximum compressive stress, σ_1, was 10.0 MPa; that of the intermediate stress, σ_2, was 6.4 MPa; and that of the minimum stress, σ_3, was 3.9 MPa. The orientations of these principal stress axes are shown in the lower hemisphere projection on the Schmidt net.

2.4. Excavation steps and AE sensor setting positions

The excavation of the chamber was started at the upper section, where rock mass was removed in the order of portions (a), (b), and (c) indicated in Fig. 4. After that, the floor was progressively excavated downward by cutting 10 benches, No. 1 through No. 10, each having a height of 3 m. Because of research budget limitations, AE monitoring was carried out during only the excavation of (1) the pillar portion in the upper section (portion (b) in Fig. 4) and (2) the No. 3 and No. 6 benches. In steps with the horizontal progress of pillar and bench excavation, AE events were monitored for 2 h immediately after each blasting near the boreholes in which the sensors were located. The symbols in Fig. 4 (a star, an open circle, and multiple crosses) indicate sources of AE events induced by these excavations.

The AE sensors were set along the three AE holes as shown in the bird's-eye view in Fig. 5. The three holes are parallel and about 3 m apart.

Each sensor consisted of a piezoelectric element and a brass case as shown in Fig. 6. The piezoelectric element, measuring 30 mm in diameter and 10 mm in thickness, was polarized in the axial direction of the disk and had a resonance frequency of 67 kHz. The piezoelectric element was placed at the bottom of a cylindrical brass case having a diameter of 40 mm and a height of 34 mm. The cylinder was then waterproofed by filling it with silicone rubber [16]. Since the dominant frequency of waveforms

actually recorded in the monitoring was in the range of 15 to 40 kHz, the resonant frequency of the sensor (including the brass case) should be within this frequency band.

Figure 7 shows a block diagram of the AE monitoring system. A signal detected at an AE sensor is first amplified by 40 dB with a pre-amplifier set in the monitoring hole and again amplified by 40 dB with a signal conditioner placed in a research shed. To eliminate noise, the signal was filtered between 5 to 100 kHz with a band-pass filter before being digitized.

3. RESULTS AND DISCUSSION

To obtain a fault-plane solution for an AE event, it is necessary to obtain clear traces of P-wave first motions at numerous sensors. Only AE events induced by large rock fractures satisfy this condition. Many AE events having small amplitudes were recorded during monitoring; however, only a small number of those events producing amplitudes sufficiently large to obtain fault-plane solutions were recorded. As shown in Table 2, we were only able to obtain fault-plane solutions for eight events: one induced during the excavation of the pillar portion, one during the excavation of the No. 3 bench, and six during the excavation of the No. 6 bench. Following the order of the events, we discuss the fracture mechanisms of these AE events in relation to stress conditions and pre-existing joint orientations.

3.1. AE event induced during the excavation of pillar portion (b)

In excavating the upper section of the underground powerhouse, two side drifts (portions (a) in Fig. 4) were driven first, after which the pillar portion (b), measuring 7 m high, 9 m wide, and 134.5 m long, was cut. Figure 8 shows a plane view detail of excavation progress of the pillar portion (b). In this detail, we see that at 10:18 on January 30, 1990, 2 m of portion (b), then in the form of a pillar, was excavated by blasting. Then, at 13:03 in the afternoon of the next day (January 31), an additional 2 m was blasted. At 13:28, 25 min after the second blasting, part of the new pillar

face (area colored black in the figure) suddenly collapsed. Simultaneous to this collapse, a large-amplitude AE event was recorded by sensors set along the three boreholes at distances of more than ten meters horizontally and vertically from the location of the collapse. From P-wave first-motion arrival times, the source was located at the position marked with a star in Fig. 8 (this location is also shown with the same symbol (a star) in the elevation view of Fig. 4 and on the bird's-eye view of Fig. 5). The collapse of the face was most likely caused by a stress concentration, because it was left in a form of a pillar tip that was easily subjected to stress concentration. From this, we infer that the AE event was induced by a sudden increase in rock stress due to stress redistribution associated with the collapse of the face.

Figure 9 shows the fault-plane solution for this AE event. The closed circle (●) indicates a sensor recording compression for P-wave first motion, while the open circle (○) indicates a sensor recording dilatation. The downward closed triangle (▼) added alongside a waveform, means that the trace of the P-wave first motion was downward, while the upward closed triangle (▲) means that the trace was upward. To check the polarity of P-wave first motion, a cap was exploded within another hole drilled in the center of and parallel to the three holes along which the AE sensors were set. Because all P-wave first motions of the traces recorded upon the cap explosion were found to be downward, the downward traces were recognized as compression, while the upward traces were recognized as

dilatation. The first motions at sensors Nos. 6 and 22 were not clear. Those at all other sensors, however, were clearly and easily classified into compression or dilatation.

Comparing the fault-plane solution to the joint orientations shown in Fig. 2, we find that the most dominant joint surface orientation (9% to 11% concentration) is around a point 68° clockwise from true north and 68° from the vertical. When we choose fault plane A in the same direction as that of the most dominant joint surface as shown in Fig. 9, the fault-plane solution thus obtained is not inconsistent. By choosing plane A as the fault plane, we can choose auxiliary plane B. From the directions of planes A and B, the P (pressure) and T (tension) axes (which indicate directions of the maximum and the minimum principal stress causing the AE event) are uniquely obtained to be in the directions shown with the letters P and T. In comparison with the stress condition shown in Fig. 3, which was measured prior to chamber excavation, we also find that the orientations of the principal stresses, σ_1 and σ_3, are similar to those of the P and T axes shown in Fig. 9.

Through the discussion, the following could be concluded: (i) the AE event was induced by a sudden increase in rock stress due to a stress redistribution associated with the partial collapse of a pillar; (ii) the AE event was induced with a fracture along one of the dominant joint surfaces; and (iii) the directions of the maximum and minimum principal stresses

causing the fracture were almost the same as those under the initial stress condition.

3.2. AE event induced by excavation of the third bench

Figure 10 shows a plane view of the progressive excavation of the No. 3 bench. Every bench, from No. 1 through No. 10, measured 3 m in height, 24 m in width and 134.5 m in length. Each bench was divided lengthwise into a 12 m penstock-side strip and a 12 m tailrace-side strip, and each respective 12 m wide strip was excavated 9-15 m along its length with each blasting. The block constituting the tailrace-side strip located immediately in front of the three holes along which the AE sensors were set was removed by blasting at 17:40, on September 15, 1990. One week later, on September 22 at 17:03, the next blasting was conducted. The No. 2 AE event discussed here was recorded 44 min after this second blasting. The location of its source is shown by an open circle (○) on the plane view (Fig. 10), on the elevation view (Fig. 4), and on the bird's-eye view (Fig. 5).

Figure 11 shows the fault-plane solution and recorded waveforms of the No. 2 AE event. The arrows added alongside the nodal planes indicate the directions of displacement deduced from the solution (in Fig. 9, it was difficult to show the displacement directions with arrows, because they were almost normal to the projection plane). Since the polarities of P-wave first motion for the AE event were readable at only six sensors, various nodal planes could conceivably be chosen to fit the data. In addition,

although the amplitudes received at sensors projected close to nodal planes should be small, those received at sensors 9 and 18 are substantial. This suggests that fracture inducing the AE event was not pure shear fracture and a vector of the displacement accompanying the fracture was not parallel to a fracture plane and had a component normal to it. If, however, the nodal planes shown in the figure are chosen, the P and T axes are both found to be almost horizontal and in directions not so different from those of the chamber axis and the borehole axis, respectively.

As shown in Fig. 10, the AE source was located at a distance only 2.6 m from the chamber wall, bordering a newly excavated 12 m wide and 30 m long opening. Thus, at the location of the AE source and as a result of the two blastings, the stress parallel the borehole axis should have decreased, while the stress perpendicular to the borehole axis (i.e., along the chamber axis) should have increased. Thus, it can be concluded that as a result of excavation, the principal stress directions of the initial stress condition shown in Fig. 3 changed to those shown with the P and T axes in the fault-plane solution. This indicates that the fault-plane solution provides useful information regarding stress redistribution due to excavation.

3.3. Six events induced by the excavation of the sixth bench

AE events Nos. 3 through 8 of Table 2 were induced by the excavation of the No. 6 bench, which was roughly 10 m lower than the level where the AE sensors were set. Figure 12 shows a plane view of the

progress of No. 6 bench excavation near the time when these events were recorded. The first blasting at 5:25, November 23, 1990, excavated a portion of the penstock side, and following it, a second blasting at 18:04 on the same day excavated a portion of the tailrace side. Within 1 min and at 32, 60, and 62 min after the second blasting, AE events of No. 3, No. 4, No. 5, and No. 6 were recorded, respectively. A third blasting was carried out the next day, November 24, at 5:37 to remove another portion on the tailrace side. At 1 and 46 min after this third blasting, AE events of No. 7 and No. 8 were recorded.

Because the magnitudes of AE events Nos. 3 through 8 were small, the polarity of the P-wave first motion could be read at only four or five sensors for each event. Due to this paucity of polarity data, it was difficult to obtain a fault-plane solution for the respective AE events. On the other hand, since the occurrence times and the located sources of the six AE events were close to each other as shown in Table 2 and Figs. 4, 5, and 12, we inferred the fracture mechanisms to be similar to each other. Thus, by superimposing the six events under the assumption that the fracture mechanisms of the AE events were the same, we obtained a fault-plane solution shown in Fig. 13.

When the two nodal planes shown in Fig. 13 were chosen, only one closed circle (●), which indicates that a sensor recorded a compressive P-wave first motion, is contained in the region where open circles (○),

which indicate sensors that recorded dilatational first motion, are otherwise exclusively distributed. This implies that nodal plane selection is not completely correct for the six events and that the respective mechanisms of the events are slight different from each other. If, however, we choose to overlook this inconsistency in the polarity of only one sensor, the fault-plane solution thereby becomes consistent for the six events.

Figure 13 shows the directions of P and T axes, together with those of the principal stresses, σ_1, σ_2, and σ_3, of the initial stress shown in Fig. 3. Although the P axis is in a similar direction to σ_1 and the T axis is in a similar direction to σ_3, the direction of the P axis is closer to vertical than that of σ_1 and the direction of the T axis is closer to horizontal than that of σ_3. This can be understood by considering that the directions of the two principal stresses turned slightly during the progressive chamber excavation. The direction of the most dominant joint surface (which shows a concentration from 9% to 11% in Fig. 2) is denoted by a broken arc in Fig. 13. We can see that the strike and dip of one of the nodal planes (N4°E/68°W) are close to those of the most dominant joint surface (N22°W/68°SW). Considering that the six AE events were recorded upon excavation of the No. 6 bench, which is around 10 m lower than the level of the No. 3 bench where the AE sensors were set, we infer that the six events were most likely caused by shear fractures slipping along the dominant joint surfaces under the influence of the in situ stress condition.

The multi-extensometer set in a hole drilled at a 22 m horizontal distance from the AE monitoring holes (see Figs. 1 and 4) measured cumulatively larger displacements toward the chamber with successive excavations of benches lower than the No. 7 bench, as shown in Fig. 14. Such large displacements were most likely caused by rock masses sliding downward along the dominant joint surfaces. Shear fractures along the dominant joint surfaces, derived from the fault-plane solution for the six AE events recorded with excavations of the No. 6 bench, seem to be a precursor to the larger displacements induced by bench excavations below the No. 7 bench. These results suggest that we can predict large rock mass sliding, a serious concern for chamber stability, if we can obtain fault-plane solutions in real time with information on the directions of dominant joint surfaces and the initial stress condition.

4. CONCLUDING REMARKS

We monitored AE events induced by the progressive excavation of a large underground chamber 280 m below the surface through the use of sensitive, high-frequency monitoring (15 to 40 kHz) for small AE events within a relatively small region. Although large AE events were seldom induced, as expected, some smaller AE events were successfully located and their fracture mechanisms were identified. Upon a discussion of fault-plane solutions together with such related considerations as the directions of dominant joint surfaces, the initial stress condition, and the shape of excavated openings around the location of the AE event, we arrive at the following conclusions.

(1) The fault-plane solution of an AE event induced by a sudden collapse of a pillar face remaining in the upper section of the chamber indicated that the AE event was induced with shear fracture along one of the dominant joint surfaces and that the directions of the maximum and minimum principal stresses causing the fracture were almost the same as those in the initial stress condition.

(2) The fault-plane solution of the AE event induced by the third bench excavation suggested that the directions of its P and T axes were strongly affected by an opening newly excavated in front of where the AE event was induced. This indicates that the fault-plane solution provides

useful information regarding stress redistribution due to excavation.

(3) The fault-plane solution obtained by superimposing the six AE events induced by the No. 6 bench excavations indicates that the six events were most likely caused by shear fracture slippage along dominant joint surfaces under the influence of in situ stress conditions. The multi-extensometer measured cumulatively large displacements toward the chamber with excavations of the benches below the No. 7 bench. The large displacements thus observed were most likely caused by rock masses sliding downward along dominant joint surfaces. The six AE events recorded with excavations of the No. 6 bench seemed to be a precursor to large displacement. The results suggest that we can predict large rock mass sliding, a serious concern for chamber stability, if we can obtain fault-plane solutions with information on the directions of dominant joint surfaces and initial stress conditions.

(4) The above discussion suggests that, by employing sensitive, high-frequency AE monitoring, fault-plane solutions can be effectively utilized as a tool for assessing the stability of a chamber carefully excavated at shallow depth with sufficient reinforcement, as well as in deep mines where fault-plane solutions have already been used in practice to assess and control rockbursts.

Acknowledgements

We would like to thank the following people: the late Mr. Atsushi Yada of the Kansai Electric Power Company Inc.; Messrs. Masaru Urayama and Takahiro Nakamura, both of NEWJEC Inc.; and Dr. Yoshiki Nakayama, Mr. Tomoaki Munemura, and the late Dr. Masahiro Tanaka of Nihon Public Company Inc., for their assistance in providing field data and for their useful discussions of that data.

The contents of this paper will be included in the book *Microcracking in Rock as Acoustic Emission* by Tsuyoshi Ishida and Joseph F. Labuz, to be published by Taylor & Francis in 2014.

References

[1] Trifu CI, Shumila V. Reliability of seismic moment tensor inversions for induced microseismicity at Kidd Mine, Ontario. Pure Appl Geophys 2002; 159: 145-64.

[2] Linzer LM. A relative moment tensor inversion technique applied to seismicity induced by mining, Rock Mech Rock Eng 2005; 38(2): 81–104.

[3] Julià J, Nyblade AA, Durrheim R, Linzer L, Gök R, Dirks P, Walter W. Source mechanisms of mine-related seismicity, Savuka Mine, South Africa, Bull Seism Soc Am 2009; 99(5): 2801-14.

[4] Bischoff M, Cete A, Fritschen R, Meier T. Coal mining induced seismicity in the Ruhr area, Germany, Pure Appl Geophys 2010; 167: 63-75.

[5] Alber M, Fritschen R, Bischoff M, Meier T. Rock mechanical investigations of seismic events in a deep longwall coal mine, Int J Rock Mech Min Sci 2009; 46: 408-20.

[6] Stec K. Characteristics of seismic activity of the Upper Silesian Coal Basin in Poland, Geophys J Int. 2007; 168: 757-68.

[7] Baker C, Young RP. Evidence for extensile crack initiation in point source time-dependent moment tensor solutions, Bull Seism Soc Am 1997; 87(6), 1442-53.

[8] Young RP, Collins DS, Reyes-Montes JM, Baker C. Quantification and interpretation of seismicity, Int J Rock Mech Min Sci 2004; 41: 1317-27.

[9] Feignier B, Young RP. Moment tensor inversion of induced microseismic events: Evidence of non‐shear failures in the -4<M <-2

moment magnitude range, Geophys Res Lett 1992; 19: 1503-6.

[10] Cai M, Kaiser PK, Morioka H, Minami M, Maejima T, Tasaka Y, Kurose H. FLAC/PFC coupled numerical simulation of AE in large-scale underground excavations, Int J Rock Mech Min Sci 2007; 44: 550-64.

[11] Ishida T, Kanagawa T, Kanaori Y. Source distribution of acoustic emission during an *in-situ* direct shear test: Implication for an analog model of inhomogeneous rock-mass fracturing, Eng Geol 2010; 110: 66-76.

[12] Ishida T, Kitano K, Kinoshita N, Wakabayashi N. Acoustic emission monitoring during in-situ heater test of granite, J Acoust Emiss 1991/92;10(1-2): S42-8.

[13] Ishida T. Acoustic emission monitoring of hydraulic fracturing in laboratory and field, Constr Build Mater 2001;15: 283-95.

[14] Ishida T, Kanagawa T, Uchita Y. Urayama M. Fault-plane solutions of microseismicity induced by progressive excavations of a large underground chamber, In: Proceedings of Third International Symposium on Rockburst and Seismicity in Mines, Kingston, 1993, p.195-8.

[15] Ishida T, Kanagawa T, Uchita Y, Urayama M. Acoustic emission mechanism and rock mass behavior as deduced from in situ measurements during progressive excavation of an underground powerhouse, In: Proceedings of the Eighth International Congress on Rock Mechanics, Tokyo, 1995. p. 593-6.

[16] Ishida T, Kanagawa T, Tsuchiyama S, Momose Y. High frequency AE monitoring with excavation of a large chamber, In: Proceeding of the Fifth Conference on Acoustic Emission/Microseismic Activity in Geologic

Structures and Materials, (held at The Pennsylvania State University at June 1991), 1995, p.479-90.

[17] Ishida T, Uchita Y. Strain monitoring of borehole diameter changes in heterogeneous jointed wall rock with chamber excavation; estimation of stress redistribution, Eng Geol 2000; 56(1-2): 63-74.

[18] Shah KR, Labuz JF. Damage mechanisms in stressed rock from acoustic emission, J Geophys Res 1995; 100(B8): 15527-39.

[19] Barton N, Lien R, Lunde J. Engineering classification of rock masses for the design of tunnel support. Rock Mech 1974; 6 (4): 189–236.

[20] Kanagawa T, Hibino S, Ishida T, Hayashi M, Kitahara Y. In situ stress measurements in the Japanese Islands: overcoring results from a multi-element gauge used at 23 sites. Int J Rock Mech Min Sci Geomech Abstr 1986; 23 (1): 29–39.

[21] Kanagawa T, Hibino S, Ishida T. In situ stress measurements by the overcoring method, development of an 8-element gauge for 3-dimensional estimation. Central Research Institute of Electric Power Industry (CRIEPI) Report, 1988, EU88002.

[22] Vutukuri VS, Katsuyama K. Introduction to rock mechanics. Tokyo: Industrial Publishing & Consulting, Inc; 1994, p.155-156.

[23] Harada M, Katayama T, Yada A. Design and construction of chamber for an underground powerhouse for Ohkawachi hydroelectric power station. Electric Power Civil Engineering 1991; 230, 46-57. (in Japanese)

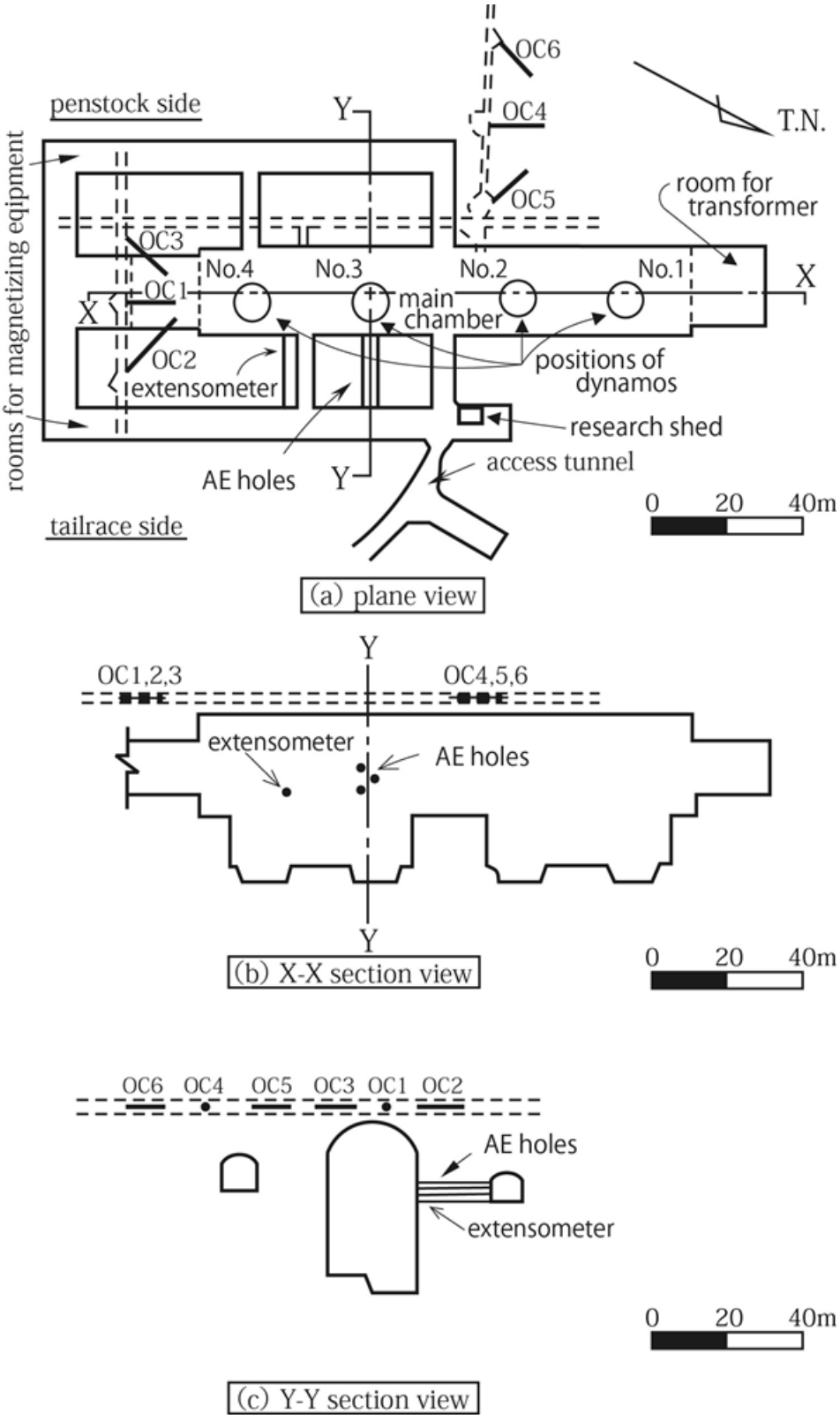

Figure 1. Underground powerhouse layout; position of holes for AE monitoring

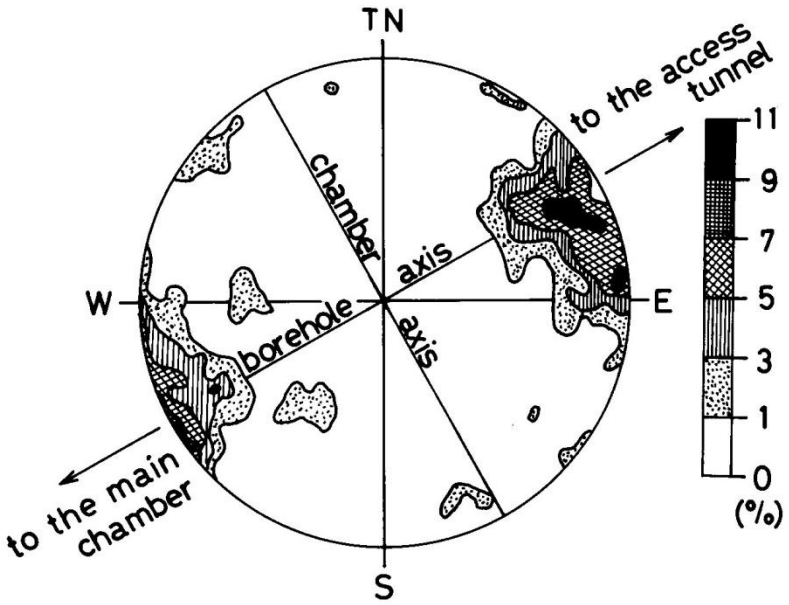

Figure 2. Lower hemisphere projection of joint surface orientations on Schmidt net

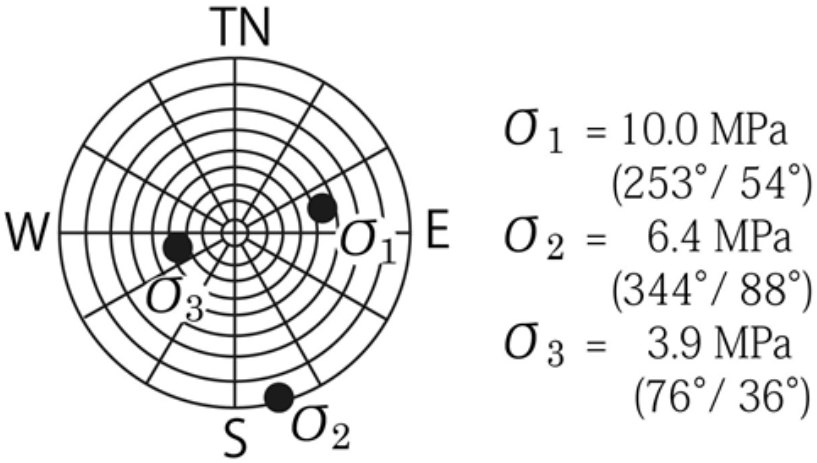

Figure 3. In situ stress condition measured by an over-coring method before main chamber excavation

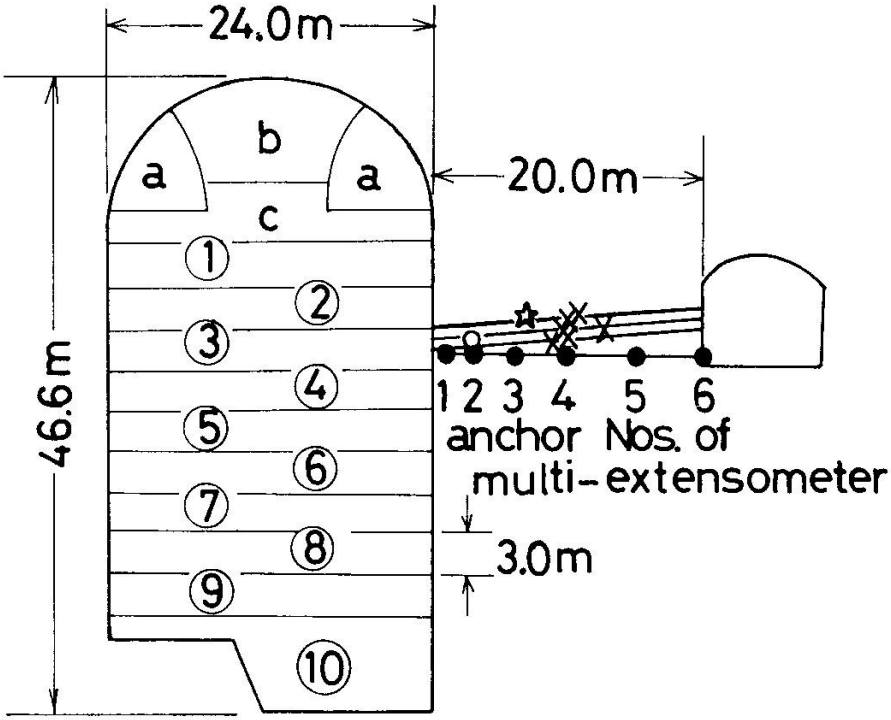

Figure 4. Elevation view: excavation steps for main chamber; AE sensor holes; multi-extensometer anchor position. Star, open circle, and crosses indicate locations of AE sources

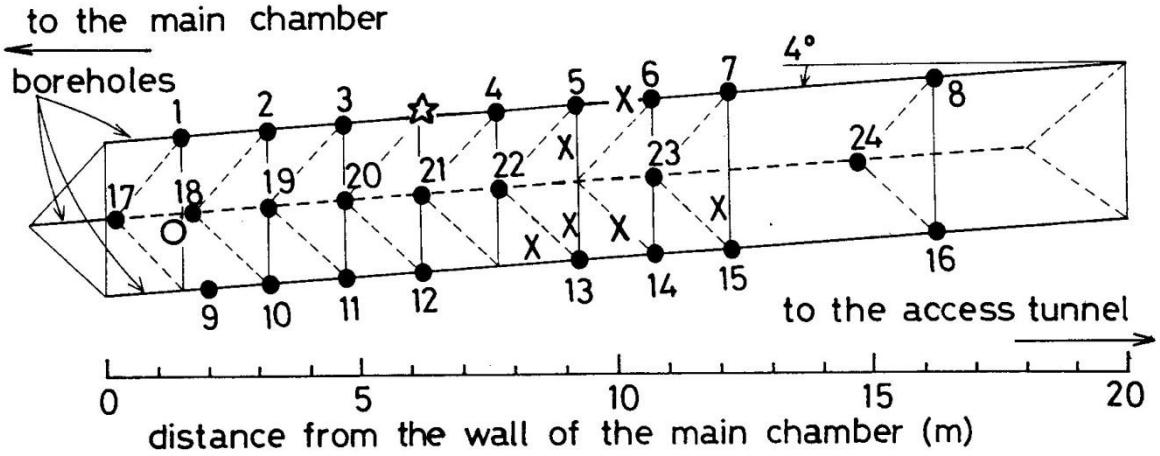

Figure 5. Bird's-eye view: arrangement of AE sensors; locations of AE sources

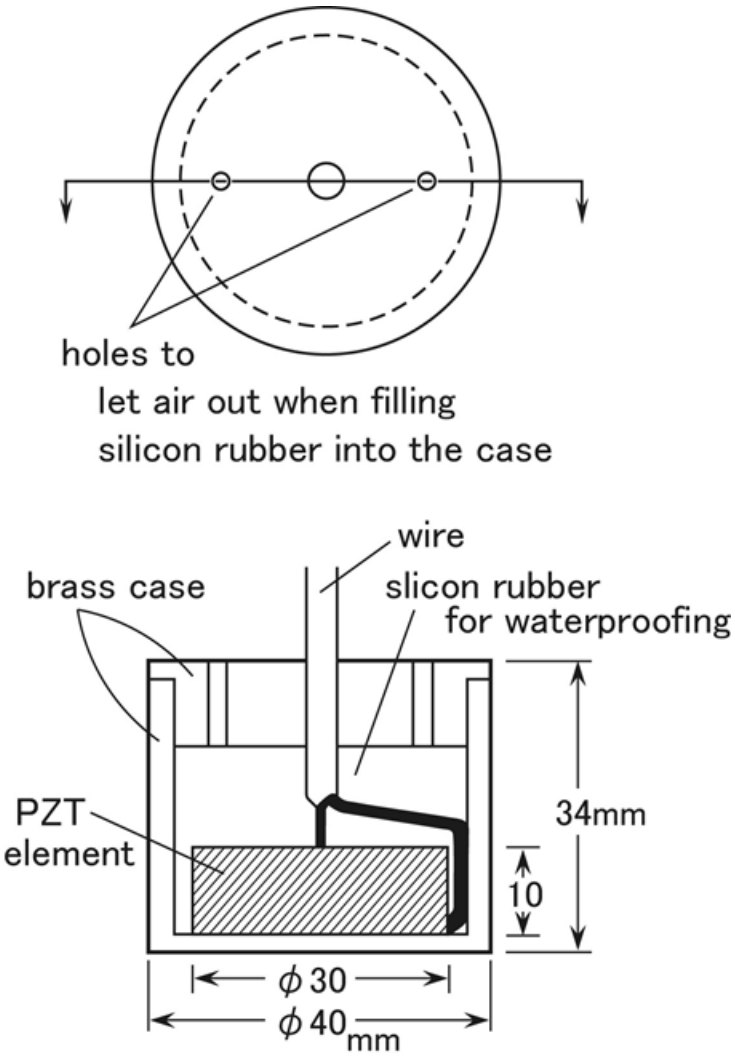

Figure 6. Plane and sectional views: AE sensor

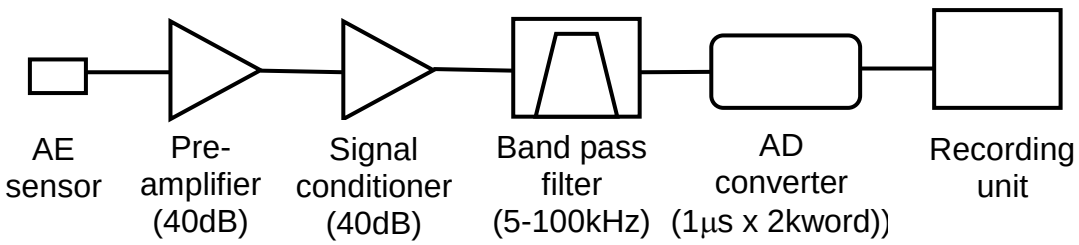

Figure 7. Block diagram: AE monitoring system

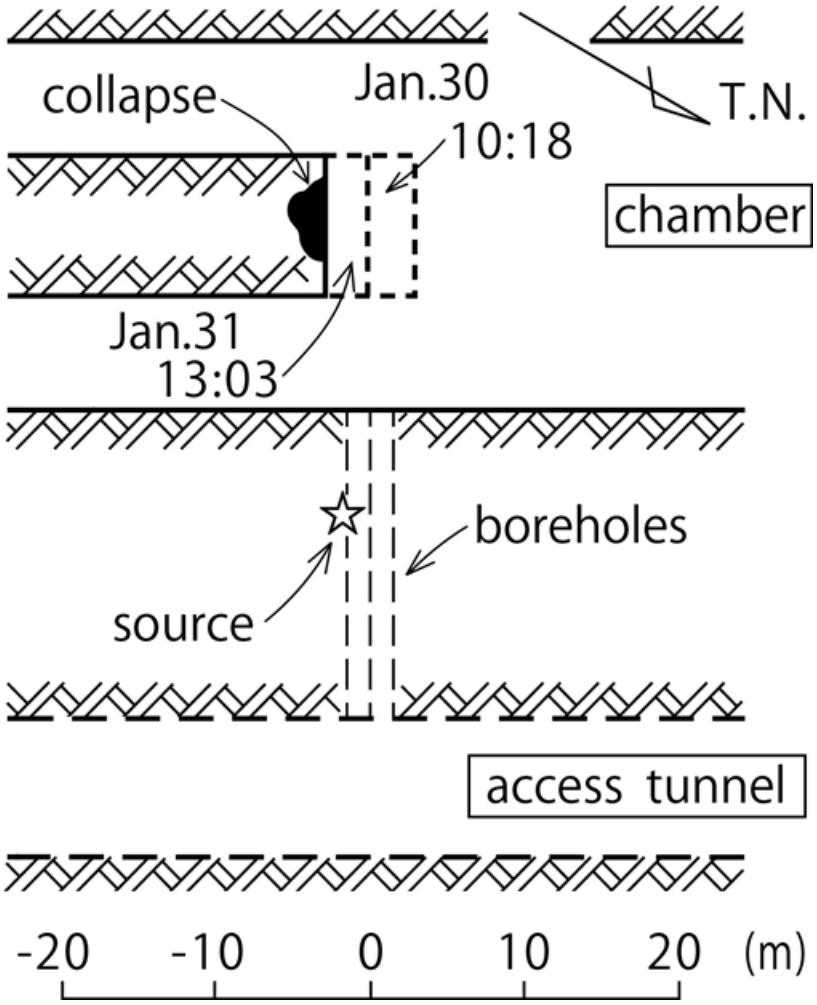

Figure 8. Plane view: progressive excavations in an upper section of the chamber just before AE event No. 1 was recorded

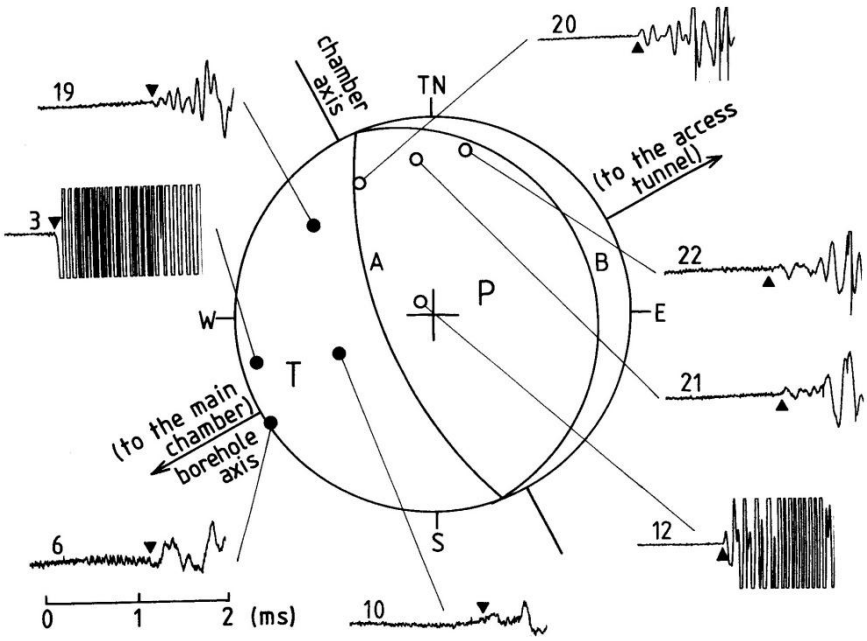

Figure 9. Fault-plane solution of No. 1 AE event (lower hemisphere projection of Schmidt net) and recorded waveforms

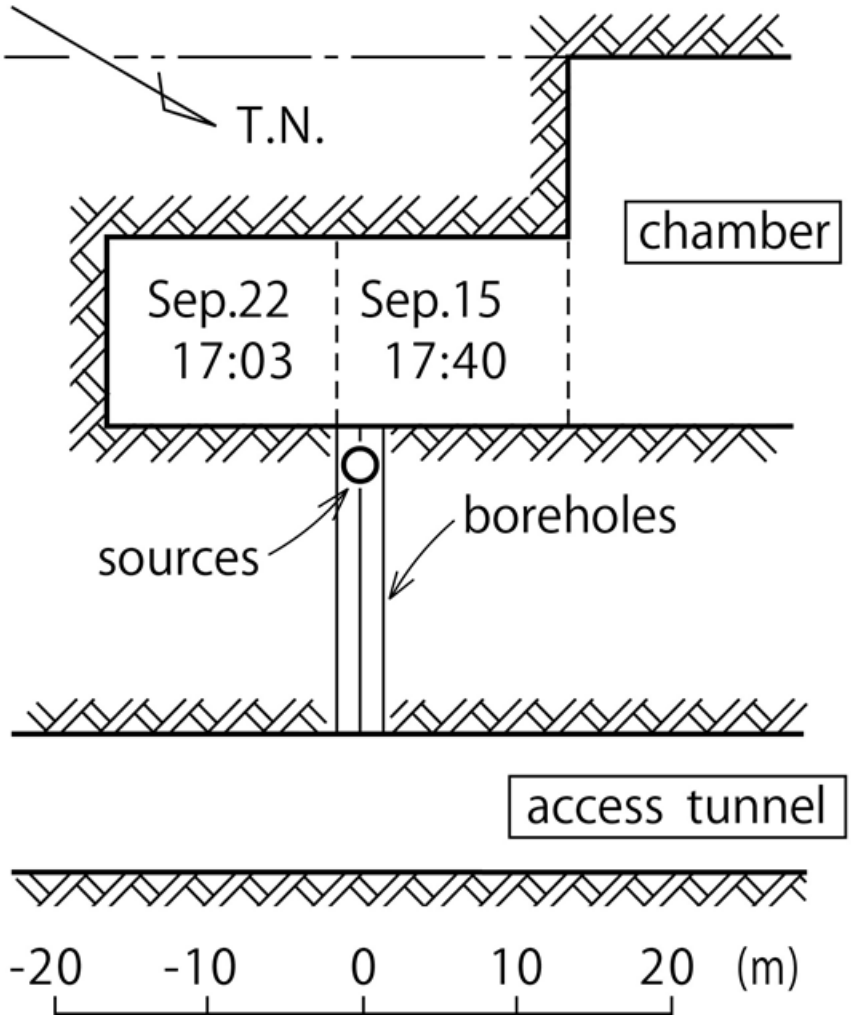

Figure 10. Plane view: progressive excavations of No. 3 bench just before AE event No. 2 was recorded

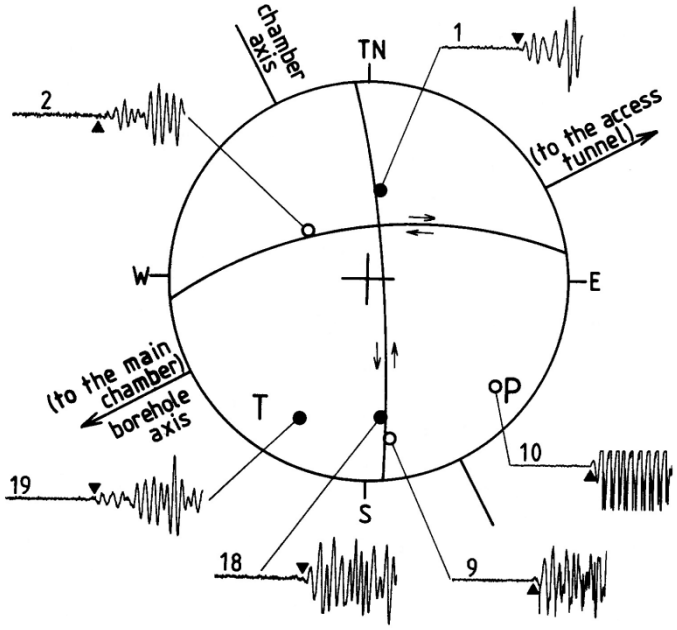

Figure 11. Fault-plane solution of the No. 2 AE event and recorded waveforms

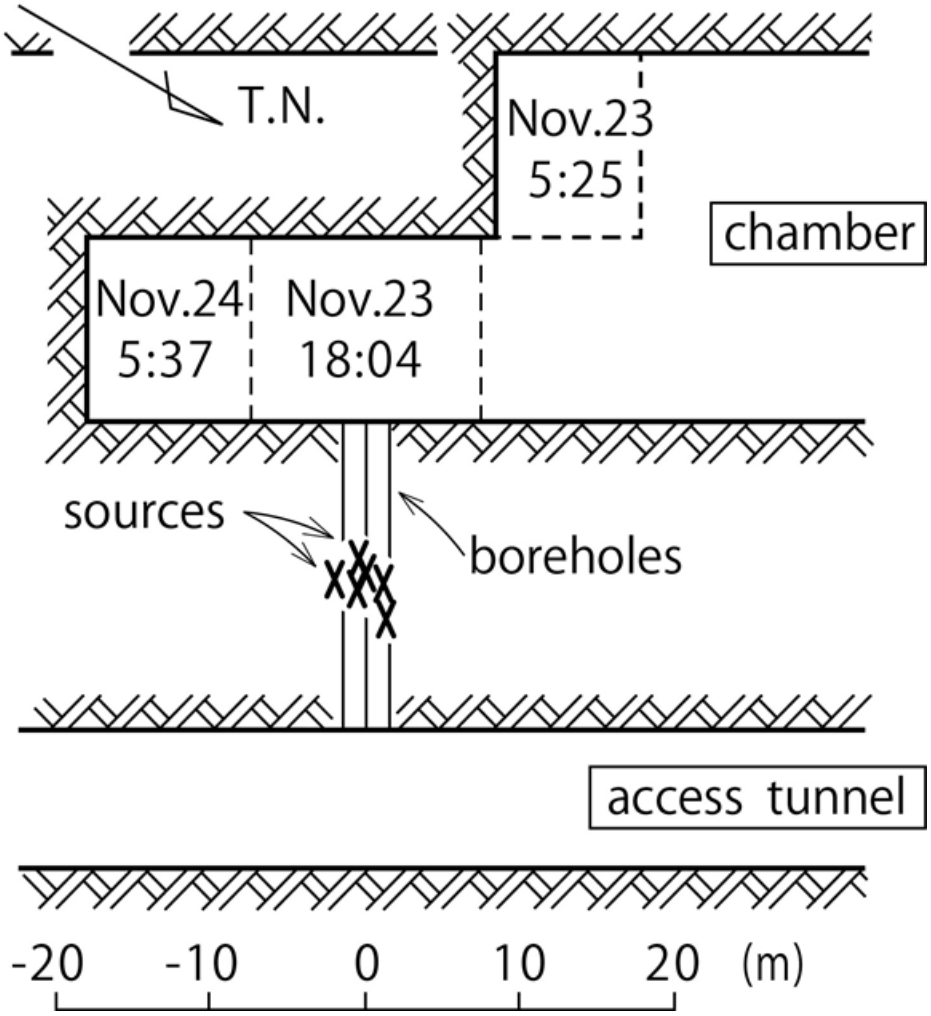

Figure 12. Plane view: progressive excavations of No. 6 bench near the when AE events Nos. 3 through 8 were recorded

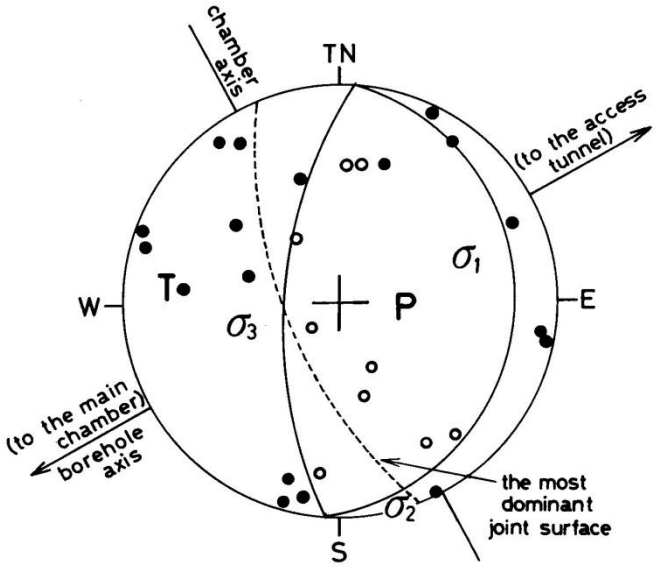

Figure 13. Fault-plane solution obtained by superimposing the polarity distributions of AE events Nos. 3 through 8

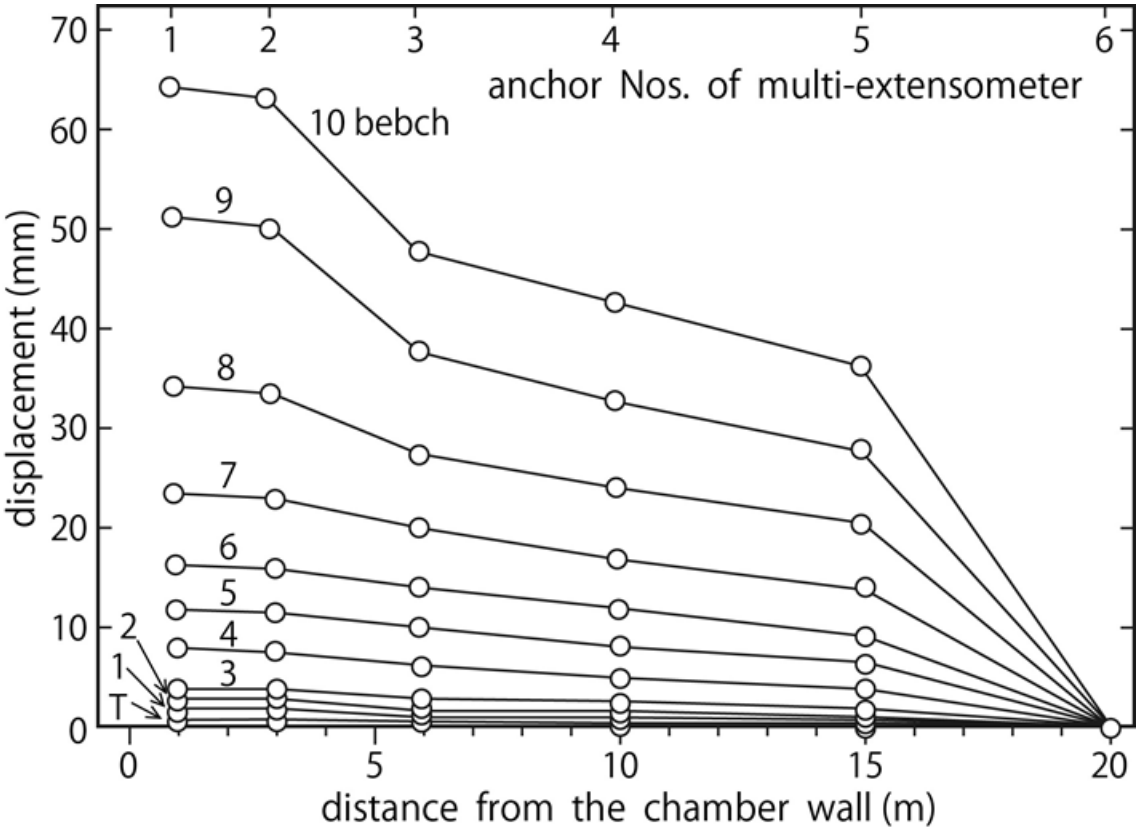

Figure 14. Horizontal displacements measured by multi-extensometer

Table 1. Mechanical properties of porphyritic rock at the Ohkawachi site

Mechanical properties	Mean value	Numbers of data
Intact (laboratory)		
Specific gravity	2.75	69
Water absorption (%)	0.34	69
Unconfined compressive strength (MPa)	236.7	76
Tensile strength (MPa)	11.8	49
Young's modulus (GPa)	76	71
Poisson ratio	0.25	31
P wave velocity (km/s)	5.71	36
S wave velocity (km/s)	3.69	36
Critical strain (%)	0.3	69
Rock mass *(in situ)*		
Young's modulus (GPa)	24	18
P wave velocity (km/s)	5–6	–
Shear Strength (MPa)	4.53	–
Internal friction angle (º)	60.9	–

Table 2. AE events

Event no.	Excavation	Date (1990)	Time of explosion	Time of event	Symbol
1	b (upper part)	Jan. 31	13:03	13:28	☆
2	No. 3 bench	Sep. 22	17:03	17:47	○
3	No. 6 bench	Nov. 23	18:04	18:04	×
4				18:36	×
5				19:04	×
6				19:06	×
7		Nov. 24	5:37	5:38	×
8				6:23	×